Electronic Supplementary Material (ESI) for Journal of Materials Chemistry A.
This journal is © The Royal Society of Chemistry 2018

Supporting Information for

Synergistic effect of P-doping and MnO_2 cocatalyst on hematite nanorod photoanode for efficient solar water splitting

Qiang Rui[a,b], Lei Wang[a], Yajun Zhang[a], Chenchen Feng[a], Beibei Zhang[a], Shurong Fu[a], Huilin Guo[b], Hongyan Hu[a,*], and Yingpu Bi[a,*]

[a] State Key Laboratory for Oxo Synthesis & Selective Oxidation, National Engineering Research Center for Fine Petrochemical Intermediates, Lanzhou Institute of Chemical Physics, CAS, Lanzhou (Gansu), 730000, China

E-mail: yingpubi@licp.cas.cn; huhongyan@licp.cas.cn.

[b] Key Laboratory of Synthetic and Natural Functional Molecule Chemistry (Ministry of Education), College of Chemistry and Materials Science, Northwest University, Xi'an, 710127, China.

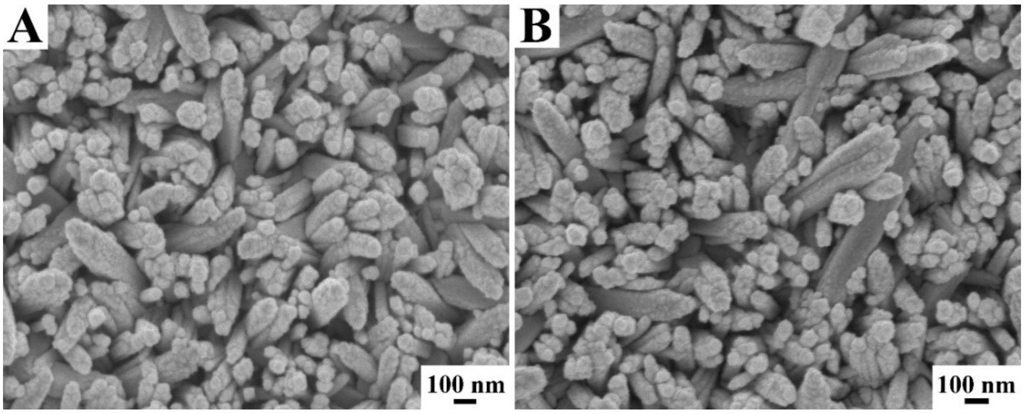

Fig. S1 SEM images of (A) P: Fe_2O_3 and (B) MnO_2/Fe_2O_3.

Results and discussions

Fig. S1 shows the typical SEM images of the P-doped and MnO_2 modified Fe_2O_3, respectively. As compared with the pristine Fe_2O_3 nanorods shown in Fig.1A, no evident structural or morphological change has been observed with P-doping or MnO_2 modification.

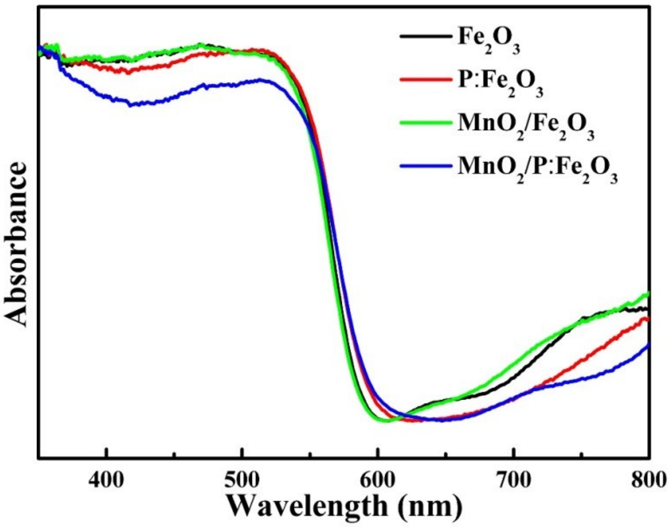

Fig. S2 UV-vis spectra of Fe_2O_3, P: Fe_2O_3, MnO_2/Fe_2O_3 and MnO_2/P: Fe_2O_3 photoanodes.

Results and discussions

The UV-vis absorption spectra were measured to study the absorption band edge of different photoanodes (Fig. S2). It can be seen that with the MnO_2 loading, the absorption spectra has no evident change compared with pristine Fe_2O_3. However, after P-doping treatment, the absorption band edge has a slight red-shift, indicating that P-doped could slightly enhance the visible light absorption.

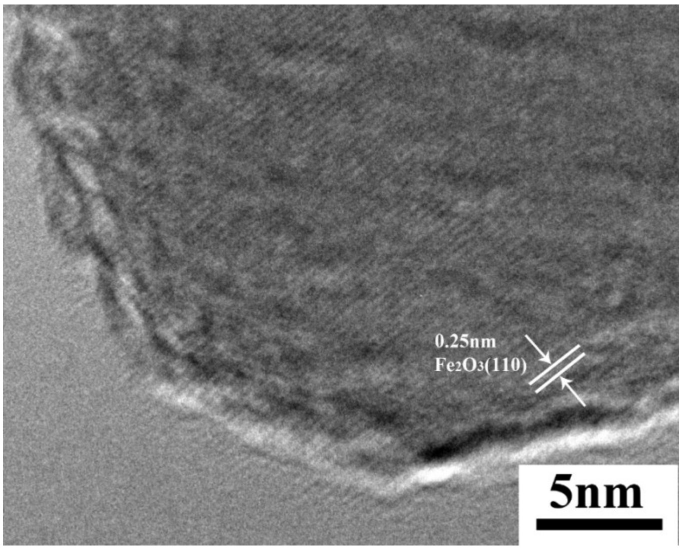

Fig. S3 HR-TEM image of Fe_2O_3.

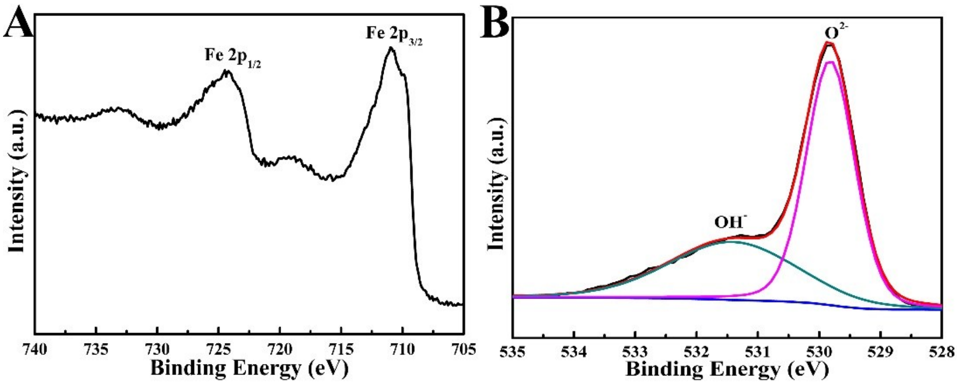

Fig. S4 XPS spectra of Fe_2O_3: (A) Fe 2p and (B) O 1s.

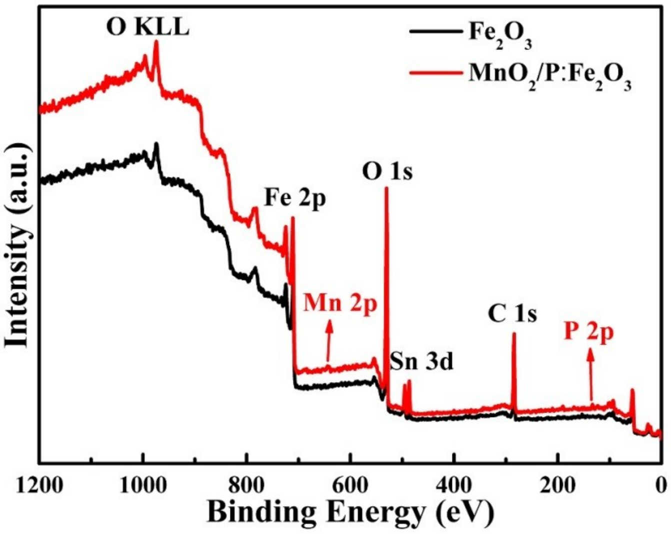

Fig. S5 XPS survey spectra of Fe_2O_3 (black) and MnO_2/P: Fe_2O_3 (red).

Results and discussions

The survey spectrum of the Fe_2O_3 and MnO_2/P: Fe_2O_3 has been compared in Fig.S5. It can be found that except for the P and Mn elements resulted from P-doping and MnO_2 modification, no additional element has been detected in the XPS spectrum. The doping content of P element in MnO_2/P: Fe_2O_3 photoanode was about 2%, which was calculated from the peak areas of XPS spectra.

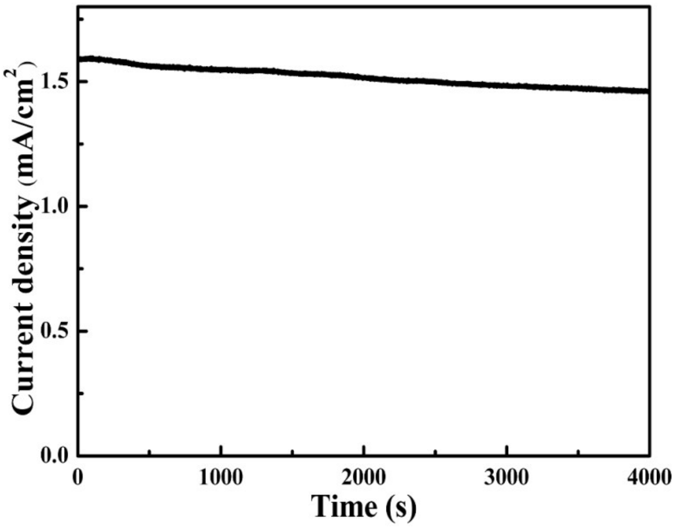

Fig. S6 Stability test of MnO_2/P: Fe_2O_3 photoanode for 4000s at 1.23V_{RHE} under AM 1.5G illumination.

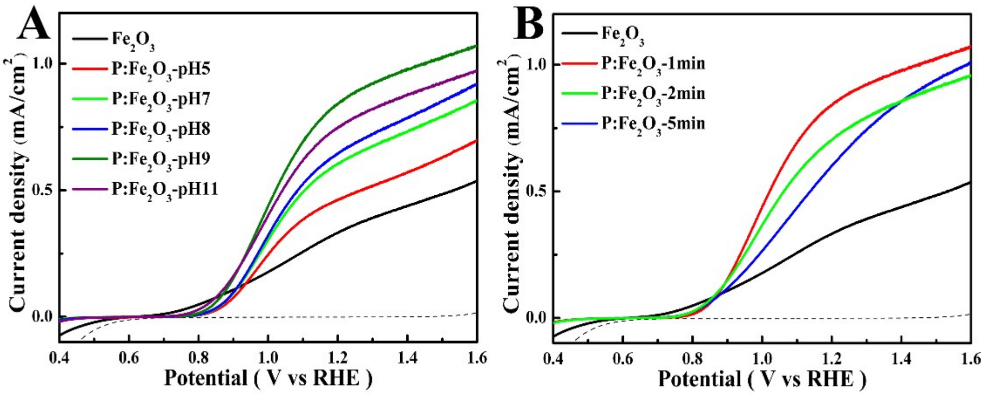

Fig. S7 J-V curves of P: Fe_2O_3 photoanodes with (A) different pH of Na_2HPO_4 solution and (B) different immersion time of Na_2HPO_4 solution.

Results and discussions

The P-doping have been further optimized by adjusting the pH values as well as the immersion time of phosphorus precursor. It can be seen from Fig. S7A, as the pH values of Na_2HPO_4 solution increased from 5 to 11, the photocurrent density increased and reached a maximum at the pH value of 9. Further increasing the pH value to 11, the PEC performances gradually decreased. Moreover, the effects of immersion time of Na_2HPO_4 solution (pH9) on the PEC properties have also been studied. As shown in Fig. S7B, the optimal photocurrent density has been achieved at the immersion time of 1min. Based on the above results, it can be concluded that with rationally tailoring the P-doping, the optimized PEC activities could be obtained. These results as well as related discussions have been added in the revised supporting information.

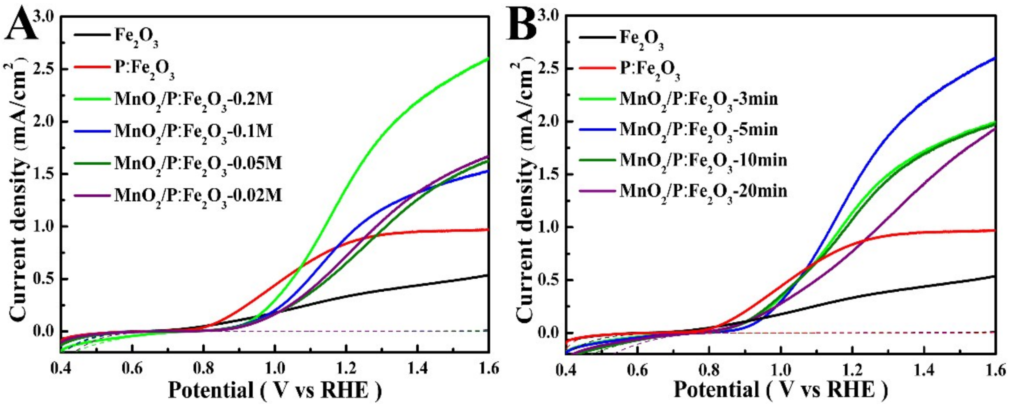

Fig. S8 J-V curves of MnO_2/P: Fe_2O_3 photoanodes with (A) different concentration of $KMnO_4$ solution and (B) different immersion time of $KMnO_4$ solution.

Results and discussions

Besides, we optimize the conditions for the modification of MnO_2, including the concentration and the immersion time of $KMnO_4$ solution. As the concentration of $KMnO_4$ solution increased from 0.02 to 0.2 M, the photocurrent density correspondingly increased, reaching the maximum at 0.2M (Fig. S8A). However, the tendency for the immersion time of $KMnO_4$ solution was different from the concentration. With increasing immersion time from 3min to 20min, the photocurrent density reached the highest value at 5 min and then gradually decreased (Fig. S8B). In summary, when the concentration of $KMnO_4$ solution is 0.2M, and the immersion time is 5min, the effect of MnO_2 modification is the best.

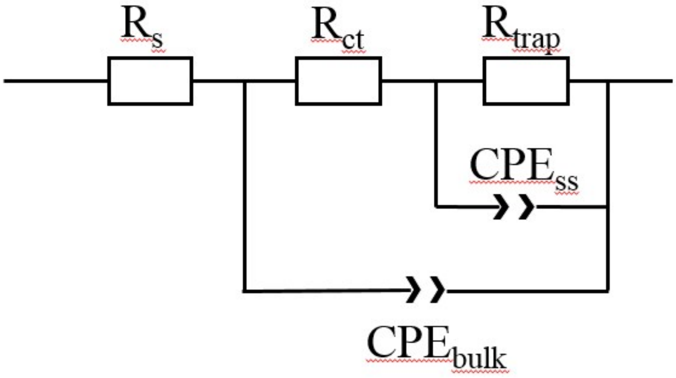

Fig. S9 Equivalent circuit model of EIS for the photoanodes.

Table S1 EIS fitting results of R_{trap} and R_{ct} for Fe_2O_3, P: Fe_2O_3, MnO_2/Fe_2O_3 and MnO_2/P: Fe_2O_3 photoanodes.

Sample	Fe_2O_3	P: Fe_2O_3	MnO_2/Fe_2O_3	MnO_2/P: Fe_2O_3
$R_{trap}(\Omega)$	705	461.7	426.8	122
$R_{ct}(\Omega)$	907.5	91.05	523	34.69

R_{trap} represents the resistance across the semiconductor/ electrolyte interface, R_{ct} represents the resistance in the Fe_2O_3.

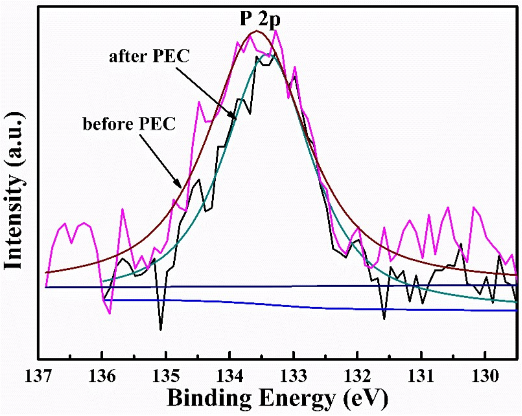

Fig. S10 P 2p XPS spectra of MnO_2/P: Fe_2O_3 before and after PEC text.

Results and discussions

XPS characterizations on MnO_2/P: Fe_2O_3 photoanodes before and after PEC tests have been performed and shown in Fig. R1. Both P_{2p} peaks with the large noises have been observed as a result of relatively low amounts of P-doping. Moreover, as compared with the fresh sample, the intensity of P_{2p} has a slight decrease, which may be due to the weak solubility of P species during the PEC tests.

Additional discussions for Figure 4

As shown in the EIS data (Fig. 4A, Table S1), the modification of MnO_2 cocatalyst can significantly reduce R_{trap} (the charge resistance across the semiconductor/electrolyte interface), indicating that MnO_2 cocatalyst could enhance hole transport for OER reaction. Moreover, it can be clearly seen from Fig. 4C shows that the modification of MnO_2 cocatalyst can effectively promote surface charge separation. Thereby, owning to the increased surface charge separation and enhanced hole migration, the significant improvement of PEC performance for water oxidation has been achieved.

It can be clearly seen from the Figure 4A that in the low potential range (0.9-0.95 V_{RHE}), the surface separation efficiency ($\eta_{surface}$) of MnO_2/P: Fe_2O_3 is slightly lower than that of pristine Fe_2O_3, which should be due to the synergistic effects of P-doping and MnO_2 cocatalyst. More specifically, although P-doping can significantly reduce the charge transfer resistance in the Fe_2O_3 for improving the conductivity, but the P sites could also serve as the recombination center for photogenerated electron-hole. Thereby, the modification of MnO_2 cocatalyst with low conductivity may further enhance the recombination of electron-hole in the low potential range. In the high potential range (1.5-1.6 V_{RHE}), the surface separation efficiency ($\eta_{surface}$) of P: Fe_2O_3 is slightly lower than that of pristine Fe_2O_3, which should be due to the slight solubility of surface P species under high potential, resulting in the charge recombination on the surface. As shown in Figure 4B, the bulk separation efficiency (η_{bulk}) of MnO_2/ Fe_2O_3 is lower than that of pristine Fe_2O_3 under low bias. Herein, we considered that the modification of MnO_2 cocatalyst with low conductivity may enhance the recombination of electron-hole in the low potential range, thus inhibiting bulk phase charge separation.